

Experimental observation of hydrodynamic-like behavior in 3D topological semimetal ZrTe₅

Chang-woo Cho^{1,2}, Peipei Wang¹, Fangdong Tang¹, Sungkyun Park²,
Mingquan He³, Rolf Lortz⁴, Qiang Li⁵, Genda Gu⁵, and Liyuan Zhang^{1,+}

¹*Department of Physics, Southern University of Science and Technology, Shenzhen 518055,
China*

²*Department of Physics, Pusan National University, Busan 46241, South Korea*

³*Low Temperature Physics Lab, College of Physics & Center of Quantum Materials and
Devices, Chongqing University, Chongqing 401331, China*

⁴*Department of Physics, The Hong Kong University of Science and Technology, Clear Water
Bay, Kowloon, Hong Kong*

⁵*Condensed Matter Physics and Materials Science Department, Brookhaven National
Laboratory, Upton, NY 11973, USA*

Hydrodynamic fluidity in condensed matter physics has been experimentally demonstrated only in a limited number of compounds due to the stringent conditions that must be met. Herein, we demonstrate phonon hydrodynamic-like properties in three-dimensional topological semimetal ZrTe₅ thanks to its ultrahigh-purity and intrinsic structural instability. By measuring the thermal properties in a wide temperature range, two representative experimental evidences of phonon hydrodynamics are seen in an interesting temperature window between the ballistic and diffusive regimes: a faster evolution of the thermal conductivity than in the ballistic regime and the non-monotonic temperature-dependent effective phonon mean-free-path. In addition, magneto-thermal conductivity results indicate us that charged quasiparticles, as well as phonons, may also play an important role in the hydrodynamic flow in the ZrTe₅ system.

⁺ Corresponding author: zhangly@sustech.edu.cn

In insulators, heat is mainly carried by phonons. This phonon-dominant heat conduction is described by Fourier's law, in which phonons scatter from other phonons, impurities, and boundaries [1-3]. This process takes place through the momentum-relaxing process known as Umklapp scattering (U-scattering). During this process, heat fluxes are dissipated and the crystal momentum is not conserved [1-3]. On the other hand, at a sufficiently low temperature T , Fourier's law no longer holds, where the crystal momentum is conserved thanks to the dominant Normal scattering (N-scattering) [4-6]. These two types of scattering mechanisms are known for a diffusive and a ballistic regime, respectively, and have been widely studied in many solids [7-11].

Meanwhile, Gurzhi proposed a viscous flow driven by the heat carriers when N-scattering is abundant in the overlapping two regimes [12]. Since then, it has been called hydrodynamic flow due to its analogy with macroscopic transport phenomena in water fluids. [13]. In the case where phonons represent the primary heat carriers in solids, two significant characteristics are known as Poiseuille flow and the second-sound wave [6,14]. The former is characterized by a steady-state phonon flow in which thermal resistance diffuses due to the boundary scattering combined with N-scattering [15,16]. In comparison, the latter involves wave-propagation of a T -gradient without significant attenuation [6,17,18].

Despite the fascination of hydrodynamics in solid state systems, experimental observation is rare. Moreover, it is found only in a narrow T -window at a remarkably low T , where abundant N-scattering and a suitable sample size are additionally required. For instance, the reported T -window of Poiseuille flow in suspended graphene was only 0.5 K at about 1 K. [19]. One reason for this practical difficulty is that U-scattering overwhelms N-scattering in almost every T -range except at significantly low T . For these reasons, phonon-hydrodynamic (PH) behavior has been experimentally confirmed in only a handful of compounds, such as solid He³ [20] and He⁴ [21], Bi [22], black P [16] and SrTiO₃ [23]. Therefore, the search for new materials in which hydrodynamics contributed through phonons or other collective excitations is of great interest to the condensed matter community.

In this study, we performed thermal and electrical transport experiments for topological semimetallic ZrTe₅ single crystals to investigate the hydrodynamic property. In fact, the ZrTe₅ study is initiated decades ago due to its considerable thermoelectric performance and resistivity anomaly [24,25]. Recently, it has gained renewed attention due to non-trivial topological phenomena such as a 3D quantum Hall effect [26], a quantum spin Hall effect on a monolayer [27], and a chiral magnetic effect [28]. Moreover, it has been reported that bulk ZrTe₅ sits at the boundary between a weak- and a strong-topological phase, so that an external perturbation easily affects its topology [29-31]. Herein, we present experimental evidence for PH by observing a faster evolution of the thermal conductivity κ than in the ballistic regime and a non-monotonic T -dependent effective phonon mean-free-path (MFP). In contrast to the conventional PH, we also find an unexpected thermal transport behavior in a hydrodynamic regime, which could be attributed to the charged quasiparticles. After reviewing several

scenarios, we suggest the coexistence of hydrodynamics led by both quasiparticles and phonons. Our findings have important implications for ongoing research on the various possible types of hydrodynamics, especially in a three-dimensional topological semimetal.

In the experimental setup, we used ultrahigh quality ZrTe_5 single crystals, which were grown by the tellurium flux method. Thanks to the relatively large size of the single acicular crystals ($l \times w \times t$, Sample #1: $3.20 \times 0.30 \times 0.08 \text{ mm}^3$, Sample #2: $2.90 \times 0.30 \times 0.21 \text{ mm}^3$), we were able to perform the electrical and thermal transport experiments on the same bulk samples. Details of the sample growth and structural properties can be found elsewhere [26,32,33]. In the main text, we defined the longest (shortest) dimension as along the a -axis (b -axis), corresponding to the ZrTe_3 chain (stacking layer) direction.

In the transport experiments, we performed the electrical resistivity measurements by the standard Hall bar method, using an alternating current with an amplitude of 0.01-0.1 mA and a frequency of 10-20 Hz. The magnetic field B was applied in the perpendicular direction to the ac -plane. In order to measure the thermal transport of such a needle-shaped ZrTe_5 crystal, we used a well-known steady-state method with one-heater and three-thermometers as shown in **Fig. 1c-e**. One end of a ~ 3.0 mm long sample was attached to a copper heat sink, while a small chip-like ~ 100 Ohm resistor and three well-calibrated Cernox thermometers were suspended from glass fibers. To minimize heat loss, thin Pt/W wires (25 μm) were used between all electrical devices and electrodes on the holder, while thick Ag wires (100 μm) were connected to the sample for the best thermal equilibrium state during the measurement. To eliminate spurious longitudinal (or transverse) components, we measured and averaged every transport experiments in opposite B -field directions. Since the sensitivity of the thermometers used in this study vanishes towards higher T , we switched to a thermocouple method to record the thermal gradient in the high T regime ($T > \sim 20$ K). In the overlapping range (about 10-20 K), we confirmed the consistent κ results within the error bars; an example for Sample #2 is presented in supplementary **Fig. S1**.

In the following, we will examine the first evidence of PH. In a hydrodynamic regime, κ should evolve faster than a T^3 -dependence. To test this, we plot the T -dependent total thermal conductivity κ_{tot} (open squares in Sample #1 and circles in Sample #2), and the electronic thermal conductivity κ_e (solid lines) in **Fig. 1a**. Note that only κ_{tot} is a directly measured value, whereas κ_e is extracted from the Wiedemann-Franz (WF) law ($\kappa_e = \frac{T}{\rho} L_0$, Lorenz number $L_0 = 2.44 \times 10^{-8} \text{ W}\Omega\text{K}^{-2}$) based on our electrical resistivity data. The T -dependent electrical resistivity and relevant Hall results are included in supplementary **Fig. S2**. For clarity, it is plotted on a log-log scale here. In the high T regime ($\sim 30 - 300$ K), it follows a perfect $1/T$ dependence in all the samples (dash-dot line in **Fig. 1a**), meaning that the U-scattering is the most prominent process in this range. After passing through the κ_{tot} peak, it starts to decrease,

indicating the N-scattering process begins to dominate. Sample #2 first shows a downward kink-like anomaly just below the T where the maximum occurs. With further cooling, the slope of κ_{tot} gradually increases towards low T and exceeds a T^5 dependence below ~ 2 K (dashed line in **Fig. 1a**). Although we do not find a similar kink-like anomaly in Sample #1, it shows a very similar behavior with a slightly slower increase in slope. It should be mentioned that in our case the phonon thermal conductivity κ_{ph} dominates by more than one order of magnitude across the entire T -range. In addition, the κ_{tot} must converge to κ_e at sufficiently low T , since the thermal energy at low T is mainly transferred from the charge carriers. However, we see no convergence up to the experimental low T -limit of 0.7 K. This is due to the comparatively high-purity crystallinity and extremely low carrier density at low T (see **Fig. S2b and c**), so that phonons still contribute mainly at low T . Such phonon dominant thermal transport behavior can be also evidenced by the large violation of Lorenz ratio L/L_0 , as shown in **Fig 1b**.

In **Fig. 2a**, we plot the T -dependent κ/T^3 to examine another hallmark of PH. It is well known that local extrema in this quantity should be observed in the interesting T -window between the ballistic and diffusive regimes. As can be seen, both samples represent the local minima in the middle of a hydrodynamic regime. We also illustrate such a local extremum from the T -dependence of the effective phonon MFP l_{ph} , which can be calculated by the simple relation as follow;

$$\kappa = \frac{1}{3} C_v \langle v \rangle l_{ph}$$

where C_v and $\langle v \rangle$ denote the volume-specific heat and sound group velocity, respectively [23]. To quantify l_{ph} , C_v and $\langle v \rangle$ are estimated from the first-principle calculations [34,35]. It is also pointed out that a prefactor of 1/3 is comes from the thermally isotropic materials by averaging over the whole solid angles [16,36]. However, ZrTe₅ is known for a strong thermal anisotropy [34], so we simply evaluate the l_{ph} as $\kappa/C_v \langle v \rangle$ without considering the prefactor (**Fig. 2b**). In the diffusive regime, l_{ph} increases monotonically with decreasing T and begins to saturate near the κ_{tot} maxima as usual. After saturation, it becomes shorter as T is cooled further. Strikingly, a similar anomaly as in **Fig. 2a** occurs for both samples (marked by vertical arrows). By subtracting the polynomial fitting curve (dashed line in **Fig. 2b**), we can distinguish this anomaly more clearly, as presented in the inset of **Fig. 2b**.

So far, we have shown the PH-like features with the thermal transport results. The questions that arises from our results is how PH could be realized in the semimetallic ZrTe₅ and not in an insulator. In terms of the scattering time scale, the U-scattering time grows exponentially, while the N-scattering time is given by a power law T -dependence. The boundary scattering time must lie between the two for the realization of hydrodynamic flow. Not only are these conditions hardly satisfied intrinsically, but they are also easily affected by impurities. For this reason, the hydrodynamic regime is extremely fragile and has been found in a limited number of

compounds with very narrow T -windows. On the one hand, it is pointing out that an instability of the crystal structure may increase the stability of PH by enhancing N-scattering [37,38]. The materials in which a PH was reported, such as Bi, black P, and SrTiO₃, are the supporting examples, since these were not the ultra-pure systems like pure silicon. Since ZrTe₅ has been reported to have an unstable crystal structure and topology, its physical properties can be easily tuned by changing the growth environment and other external parameters [26,30,31]. Therefore, the combination of ultra-pure limit and structural instability makes ZrTe₅ a perfectly suitable material to observe PH.

Next, we examine the B -field dependence of the thermal transport. In **Fig. 3a**, we present the longitudinal thermal conductivity κ_{xx} as a function of B -field for Sample #2, measured at 0.81 K. For comparison with the electronic part of the thermal transport, we plot it together with κ_e (red line in **Fig. 3a**). Two things are worth noting here. First, one sees a clear thermal quantum oscillation that is in complete agreement with the electronic quantum oscillations in **Fig. 3a**. Although phonons still play a dominant role up to our experimental low T limit of 0.7 K, the contribution of charged particles among thermal carriers increases when T is lower. Thus, such a distinct thermal quantum oscillation at 0.81 K is reasonable. Second, it shows a nearly independent κ_{xx} to the external B -fields. When the quantum oscillations terminate at ~ 1.5 T, κ_{xx} does not change little in a higher field regime. This is also true at higher temperatures for both samples (**Fig. S3**). This is because κ_{ph} is still a factor of 100 higher than κ_e even at a low T , where κ_{ph} does not respond to B -fields because of its charge neutrality.

Unexpected thermal behavior is seen in the T -dependent electronic thermal contribution, as shown in **Fig. 3b**. As mentioned earlier, κ_{ph} was not seriously changed by the external B -fields, so we may deduce the thermal contribution of charged quasiparticles by subtracting the $\kappa_{tot}(B)$ from the $\kappa_{tot}(0T)$. To do this, we define $\Delta\kappa = \kappa_{tot}(0T) - \kappa_{tot}(B)$, where the B -field value was chosen to be 2.4 T (5.0 T) for Sample #2 (#1). Surprisingly, this quantity shows an enormous deviation in the PH regime we observed. According to the previous work of Crossno et al., in which they reported on a deviation of κ_e with largely violated the L/L_0 at a charge neutrality point in graphene, and they argued that this is indicative of Dirac fluid [39]. Although seemingly similar to the present results (significant violation of L/L_0 and nearly charge-neutrality point), our observations are different in principle. In the case of Crossno et al., the Dirac fluid hydrodynamics occurred in the non-degenerate regime [39], but our ZrTe₅ is far away in the degenerate regime. Furthermore, they observed a recovery of L/L_0 as one moves away from the neutral point [39], but we see no recovery over the entire T -window.

To gain a deeper understanding, we carry out the thermal Hall experiment, as this could be a direct probe to study quasiparticle dynamics, but has rarely been performed in topological materials due to the difficulty of obtaining high-quality data. **Figure 4a** shows the B -fields

dependence of the thermal Hall resistivity ω_{xy} ($= \frac{wt}{l} \left(\frac{\Delta T_{xy}}{P} \right)$, where ΔT_{xy} and P denote the T gradient between two points along the transverse direction and the heating power, respectively) in a narrow B -fields range from -1 to 1 T. For a higher resolution, we recorded the data this time with a continuous field sweep mode. In the main text, only the case of Sample #1 is shown (Sample #2 data is included in supplementary **Fig. S4**). The value of ω_{xy} is close to zero regardless of the measured T . This makes sense because phonons are the primary heat carriers in our ZrTe₅ samples, so the transverse thermal gradient should not be generated under the B -fields. Interestingly, an asymmetric thermal Hall feature is found in a weak field region ($|B| < 0.1$ T), which becomes stronger as T decrease.

The degree of heat deviation can be determined from the thermal Hall angle $\tan \theta_H$. In **Fig. 4b**, $\tan \theta_H$ ($= \frac{\kappa_{xy}}{\kappa_{xx}}$) is plotted as a function of B -field at various T . The trend is not different from ω_{xy} versus B . It shows a significant deviation when the B -field is applied near zero-field and is abruptly faded in the region of higher B -fields. In **Fig. 4c**, we represent the zero-field-limit ($B \rightarrow 0$) of $\tan \theta_H / B$ (hereafter $[\tan \theta_H / B]_0$), which is proportional to the effective MFP of the quasiparticles l_{QP} [40]. The magnitude of l_{QP} can be estimated through the equation $l_{QP} = \frac{\hbar k_F \tan \theta_H}{e B}$, where \hbar is the planck constant, k_F is the Fermi wave number, and e is the electron charge [41]. Using the estimation of $k_F \approx 4 \times 10^{-3} \text{\AA}^{-1}$ in the ac -plane [26], we obtain that the l_{QP} is about 40 μm at 1.0 K, which is comparably longer than those previously reported [42-44]. This consequence also supports our extremely clean ZrTe₅ samples, so that quasiparticles travel without significant momentum loss. Another striking feature of $[\tan \theta_H / B]_0$ is the presence of a local maximum (vertical arrows in **Fig. 4c**) corresponding to T at ~ 2 K (Sample #1) and ~ 6 K (Sample #2). These are also in good agreement with the PH regime we observed. Again, the thermal Hall signal is essentially from the electronic contribution, since the neutrally charged quasiparticles are not affected by a magnetic field. Therefore, it is reasonable to say that the hydrodynamic flow in ZrTe₅ is unlikely to be due to a purely phononic attribution.

Then it is puzzling what kind of collective quasiparticles induces the hydrodynamic flow in our ZrTe₅. Although we demonstrate that the heat in ZrTe₅ is dominantly carried by the phonons, the electron-electron hydrodynamic scenario is still valid. In the results of the zero-field-limit electronic Hall-angle ($[\tan \theta_e / B]_0$, inset of **Fig. 4c**), we can test it. It increases steadily as T drops to ~ 10 K, and then saturates at low T . This means that the electron-electron scattering process below 10 K is virtually unaffected by the entire scattering system.

The next possibility is an electron-phonon fluid in which the electron-phonon scattering process is the fastest, so that their momentum can be quasi-conserved. For electron-phonon cases studied previously, the results resembled ours to some extent, since there is a large violation of

L/L_0 [45]. However, the sign of L/L_0 is at odds with the present results, implying that our system is much closer to a PH-like fluid. Moreover, we find no experimental evidence of the phonon-drag effect as they have reported. Given that none of the scenarios are likely to dominate the hydrodynamics in the present results, we cautiously suggest the coexistence of phonon and charged quasiparticle hydrodynamic flows or very weakly interaction with each other in our topological semimetal $ZrTe_5$.

In summary, the main effort of hydrodynamic studies to date has been to find the significant features where either electrons or phonons provide the primary scattering. However, all transport regimes – ballistic, hydrodynamic, and diffusive – can coexist and be coupled, making it difficult to distinguish purely quasiparticle hydrodynamic phenomena. Using ultrahigh-purity single crystals of $ZrTe_5$, we have succeeded finding the Hallmarks of the PH as well as the anomalous flow of quasiparticles, which is unexpected. This requires extended theoretical and experimental work beyond the scope of the present study.

Acknowledgement

We thank Benjamin Piot, Kitinan Pongsangangan for their enlightening discussions. C.-w. Cho is supported by BK4-program from NRF-Korea. M. He acknowledges the support by National Natural Science Foundation of China (11904040), Chongqing Research Program of Basic Research and Frontier Technology, China (Grant No. cstc2020jcyj-msxmX0263), Fundamental Research Funds for the Central Universities, China(2020CDJQY-A056, 2020CDJ-LHZZ-010, 2020CDJQY-Z006), Projects of President Foundation of Chongqing University, China(2019CDXZWL002).

Figures

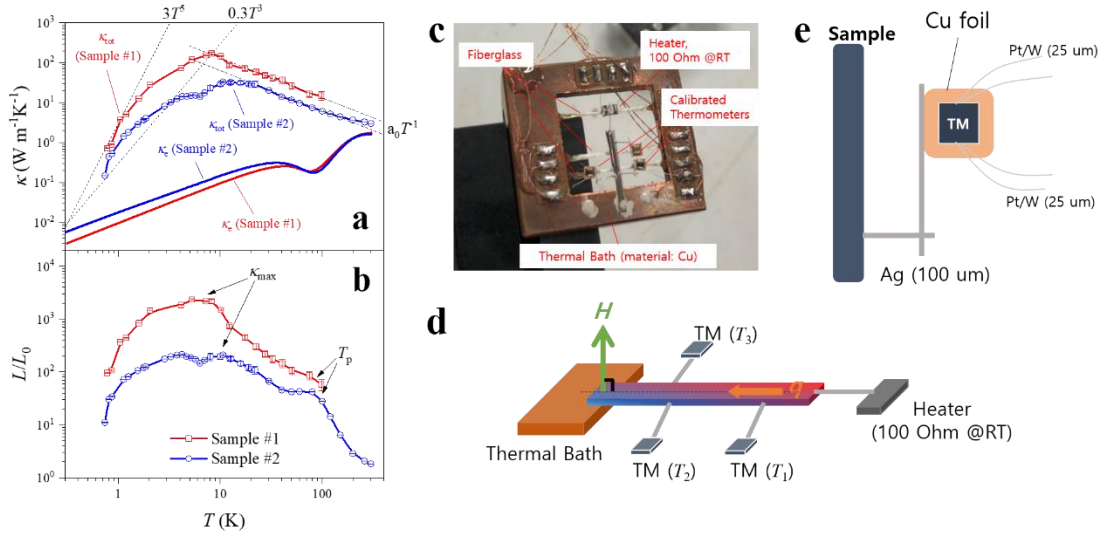


Figure 1. (a) Thermal conductivity as a function of temperature in a log-log plot for two different ZrTe₅ samples. The open squares (Sample #1) and circles (Sample #2) indicate the total thermal conductivity κ_{tot} , and the solid lines denote the charge carrier thermal conductivity κ_e , which is calculated according to the Wiedemann-Franz law ($\kappa_e = \frac{T}{\rho} L_0$, where the Lorenz number $L_0 = 2.44 \times 10^{-8} W \Omega K^{-2}$). The two dash- and dash-dot-lines proportional to T^3 , T^5 and T^{-1} are added for comparison with the T evolution of κ_{tot} . **(b)** Lorenz ratio (L/L_0) of two samples as a function of T . **(c)** Photograph of the thermal conductivity setup used in this study. **(d)** To minimize thermal leakage from the resistive heater to the thermal bath, we connected the sample to the heater and thermometers through 100 um thick Ag-wires. In comparison, the connections for the electrical measurements are made by 25 um thin Pt/W-wires since it is a good electrical conductor but a relatively poor thermal conductor. **(e)** Schematic diagram of our thermal conductivity experiment.

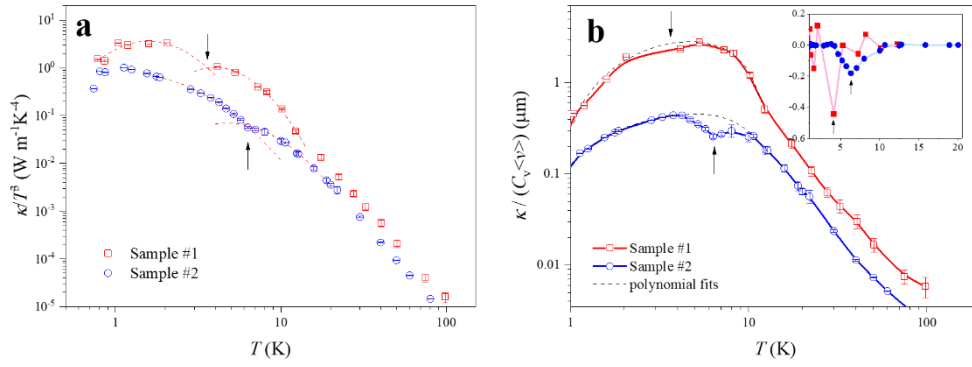


Figure 2. (a) The κ/T^3 and (b) $\kappa/C_v\langle v \rangle$ results as a function of temperature. The vertical arrows in (a) and (b) indicate the local extrema in these quantities. The dashed curves (red-color (a) and black-color (b)) are polynomial fits to clarify the kink-like anomalies. Data for which the polynomial fits have been subtracted from $\kappa/C_v\langle v \rangle$ is plotted in the inset of (b).

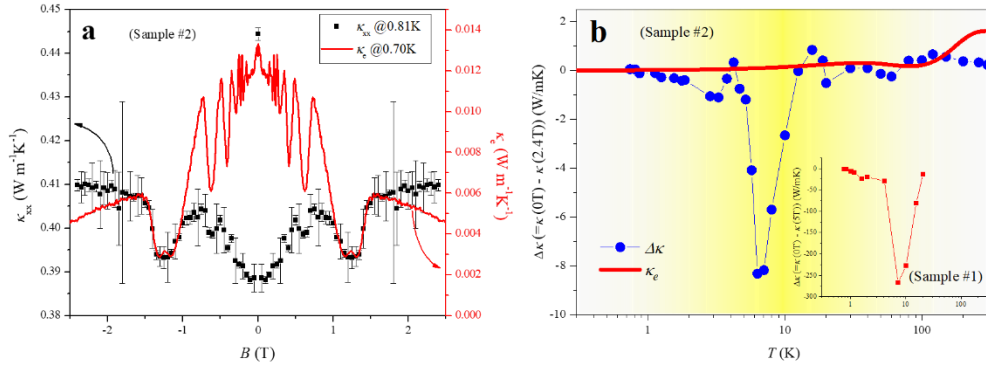


Figure 3. (a) Magnetic field dependent longitudinal total thermal conductivity κ_{xx} (closed squares) and purely electronically contributed thermal conductivity κ_e (red-solid line) measured at low temperature for Sample #2. (b) The extracted charged quasiparticles contribution to the thermal conductivity of Sample #2 (blue-closed circle). The result of Sample #1 is presented in the inset of (b). The shown κ_e (red-solid line) is calculated from the WF-law based on our electrical resistivity data. $\Delta\kappa$ strongly deviates in both samples in a hydrodynamic regime. See main text for details.

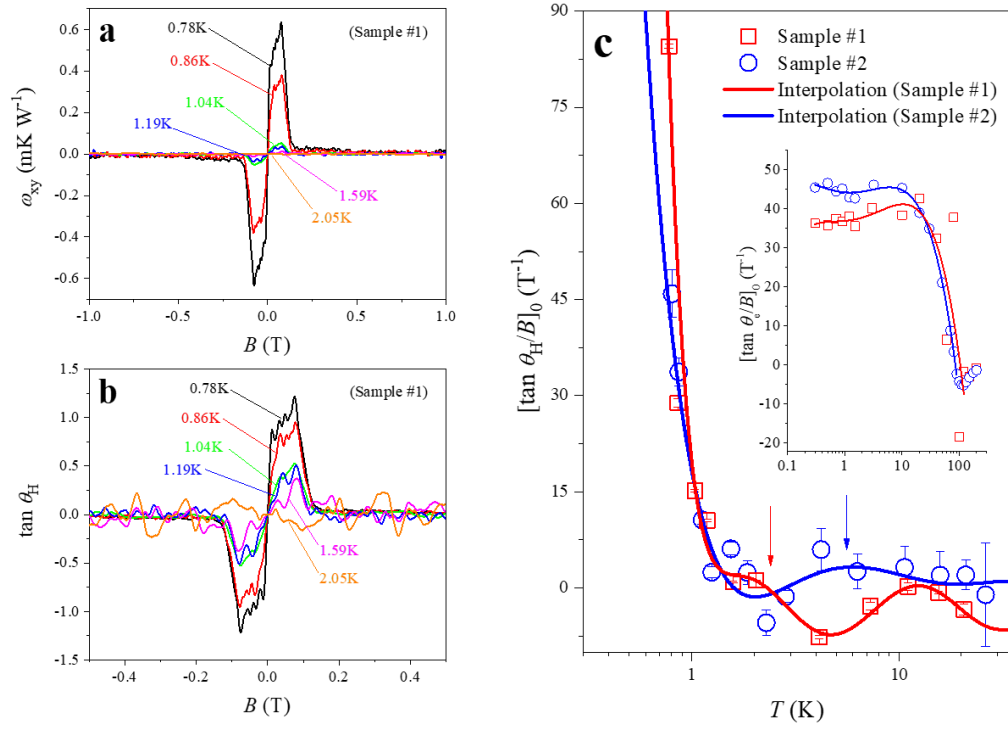


Figure 4. (a) Magnetic field dependence of the thermal Hall resistivity ω_{xy} at different temperatures (Sample #1). (b) Tangential Hall angle ($\tan \theta_H = \frac{\kappa_{xy}}{\kappa_{xx}}$) in a magnetic field range of -0.5 to 0.5 T at various temperatures (Sample #1). (c) temperature-dependent slope of $\tan \theta_H$ of B in the zero-magnetic-field-limit for two samples on a logarithmic temperature scale. In general, this value is proportional to the mean-free-path of the quasiparticles. The inset of (c) shows the initial slope of the electronic Hall angle. The vertical arrows denote the local maxima.

References

- [1] S. R. Phillpot and A. J. H. McGaughey, *Materials Today* **8 (6)**, 18 (2005).
- [2] M. Kaviany, *Principles of Heat Transfer* (Wiley, New York, 2002).
- [3] J. M. Ziman, *Electrons and Phonons: The Theory of Transport Phenomena in Solids* (Oxford Univ. Press, 2001).
- [4] M. S. Dresselhaus, G. Chen, M. Y. Tang, R. G. Yang, H. Lee, D. Z. Wang, Z. F. Ren, J.-P. Fleurial, and P. Gogna, *Adv. Mater.* **19**, 1043 (2007).
- [5] W. J. De Haas and T. Biermasz, *Physica* **4**, 752 (1937).
- [6] C. C. Ackerman, B. Bertman, H. A. Fairbank, and R. A. Guyer, *Physical Review Letters* **16**, 789 (1966).
- [7] M. Maldovan, *Applied Physics Letters* **101**, 113110 (2012).
- [8] J. Sirker, R. G. Pereira, and I. Affleck, *Physical Review Letters* **103**, 216602 (2009).
- [9] J. S. Kang, M. Li, H. Wu, H. Nguyen, and Y. Hu, *Science* **361**, 575 (2018).
- [10] M. Koch, F. Ample, C. Joachim, and L. Grill, *Nature Nanotechnology* **7**, 713 (2012).
- [11] H. M. Pastawski, *Physical Review B* **44**, 6329 (1991).
- [12] R. N. Gurzhi, *Soviet Physics Uspekhi* **11**, 255 (1968).
- [13] J. A. Sussmann and A. Thellung, *Proc. Phys. Soc.* **81**, 1122 (1963).
- [14] A. Cepellotti, G. Fugallo, L. Paulatto, M. Lazzeri, F. Mauri, and N. Marzari, *Nat. Commun.* **6**, 6400 (2015).
- [15] R. Maynard, A. Smontara, and J. C. Lasjaunias, *Physica B: Condensed Matter* **263-264**, 678 (1999).
- [16] Y. Machida, A. Subedi, K. Akiba, A. Miyake, M. Tokunaga, Y. Akahama, K. Izawa, and K. Behnia, *Sci. Adv.* **4**, eaat3374 (2018).
- [17] D. W. Pohl and V. Irniger, *Physical Review Letters* **36**, 480 (1976).
- [18] A. Koreeda, R. Takano, and S. Saikan, *Physical Review Letters* **99**, 265502 (2007).
- [19] S. Lee, D. Broido, K. Esfarjani, and G. Chen, *Nat. Commun.* **6**, 6290 (2015).
- [20] W. C. Thomlinson, *Physical Review Letters* **23**, 1330 (1969).
- [21] L. P. Mezhov-Deglin, *Soviet Physics JETP* **25**, 568 (1967).
- [22] V. N. Kopylov and L. P. Mezhov-Deglin, *Zh. Eksp. Teor. Fiz.* **65**, 720 (1973).
- [23] V. Martelli, J. L. Jimenez, M. Continentino, E. Baggio-Saitovitch, and K. Behnia, *Phys. Rev. Lett.* **120**, 125901 (2018).
- [24] S. Okada, T. Sambongi, and M. Ido, *Journal of the Physical Society of Japan* **49**, 839 (1980).
- [25] F. J. DiSalvo, R. M. Fleming, and J. V. Waszczak, *Physical Review B* **24**, 2935 (1981).
- [26] F. Tang *et al.*, *Nature* **569**, 537 (2019).
- [27] H. Weng, X. Dai, and Z. Fang, *Phys. Rev. X* **4**, 011002 (2014).
- [28] L. Y. Xiang *et al.*, *Phys. Rev. B* **94**, 094524 (2016).
- [29] Z. Fan, Q.-F. Liang, Y. B. Chen, S.-H. Yao, and J. Zhou, *Sci. Rep.* **7**, 45667 (2017).
- [30] J. Mutch, W.-C. Chen, P. Went, T. Qian, I. Z. Wilson, A. Andreev, C.-C. Chen, and J.-H. Chu, *Sci. Adv.* **5**, eaav9771 (2019).
- [31] B. Xu, L. X. Zhao, P. Marsik, E. Sheveleva, F. Lyzwa, Y. M. Dai, G. F. Chen, X. G. Qiu, and C. Bernhard, *Physical Review Letters* **121**, 187401 (2018).

- [32] Q. Li *et al.*, *Nat Phys* **12**, 550 (2016).
- [33] W. Zhang *et al.*, *Nature Communications* **11**, 1046 (2020).
- [34] J. Zhu, T. Feng, S. Mills, P. Wang, X. Wu, L. Zhang, S. T. Pantelides, X. Du, and X. Wang, *ACS Applied Materials & Interfaces* **10**, 40740 (2018).
- [35] C. Wang, H. Wang, Y. B. Chen, S.-H. Yao, and J. Zhou, *Journal of Applied Physics* **123**, 175104 (2018).
- [36] Z. Chen and C. Dames, *Applied Physics Letters* **107**, 193104 (2015).
- [37] P. B. Littlewood, *Journal of Physics C: Solid State Physics* **13**, 4855 (1980).
- [38] K. Behnia, *Science* **351**, 124 (2016).
- [39] J. Crossno *et al.*, *Science* **351**, 1058 (2016).
- [40] M. Hirschberger, J. W. Krizan, R. J. Cava, and N. P. Ong, *Science* **348**, 106 (2015).
- [41] Y. Kasahara, Y. Nakajima, K. Izawa, Y. Matsuda, K. Behnia, H. Shishido, R. Settai, and Y. Onuki, *Journal of Magnetism and Magnetic Materials* **310**, 569 (2007).
- [42] G. Zheng *et al.*, *Phys. Rev. B* **93**, 115414 (2016).
- [43] W. Wang, X. Zhang, H. Xu, Y. Zhao, W. Zou, L. He, and Y. Xu, *Scientific Reports* **8**, 5125 (2018).
- [44] P. Yang, W. Wang, X. Zhang, K. Wang, L. He, W. Liu, and Y. Xu, *Scientific Reports* **9**, 3558 (2019).
- [45] C. Fu *et al.*, *Research* **2020**, 4643507 (2020).

Supplementary Information for
Experimental observation of hydrodynamic-like behavior in 3D
topological semimetal ZrTe₅

Chang-woo Cho^{1,2}, Peipei Wang¹, Fangdong Tang¹, Sungkyun Park²,
Mingquan He³, Rolf Lortz⁴, Qiang Li⁵, Genda Gu⁵, and Liyuan Zhang^{1,+}

*¹Department of Physics, Southern University of Science and Technology, Shenzhen 518055,
China*

²Department of Physics, Pusan National University, Busan 46241, South Korea

*³Low Temperature Physics Lab, College of Physics & Center of Quantum Materials and
Devices, Chongqing University, Chongqing 401331, China*

*⁴Department of Physics, The Hong Kong University of Science and Technology, Clear Water
Bay, Kowloon, Hong Kong*

*⁵Condensed Matter Physics and Materials Science Department, Brookhaven National
Laboratory, Upton, NY 11973, USA*

⁺ Corresponding author: zhangly@sustech.edu.cn

1. Two different methods to measure the thermal conductivity: Thermometer vs Thermocouple

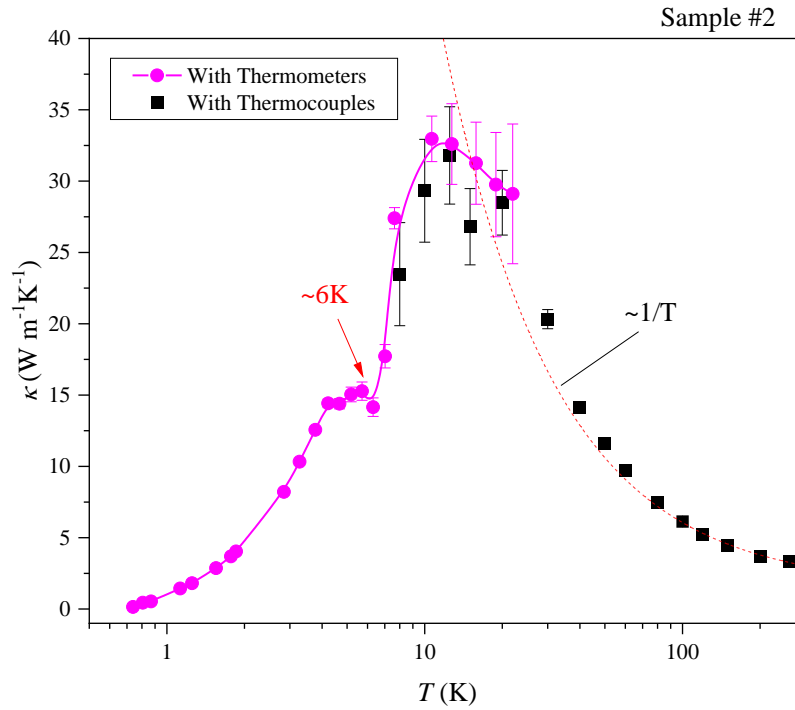


Figure S1. Thermal conductivity as a function of temperature for Sample #2. At low temperatures, thermometers were used to record the temperature gradient because of their high sensitivity originating from the semiconducting nature (magenta). On the other hand, thermocouples are more sensitive at higher temperatures (black). In our experiments, we observe the overlapping temperature range from ~ 10 to ~ 20 K. The dashed curve (red) denotes the $1/T$ dependence curve.

2. Temperature dependent electrical resistivity and Hall results

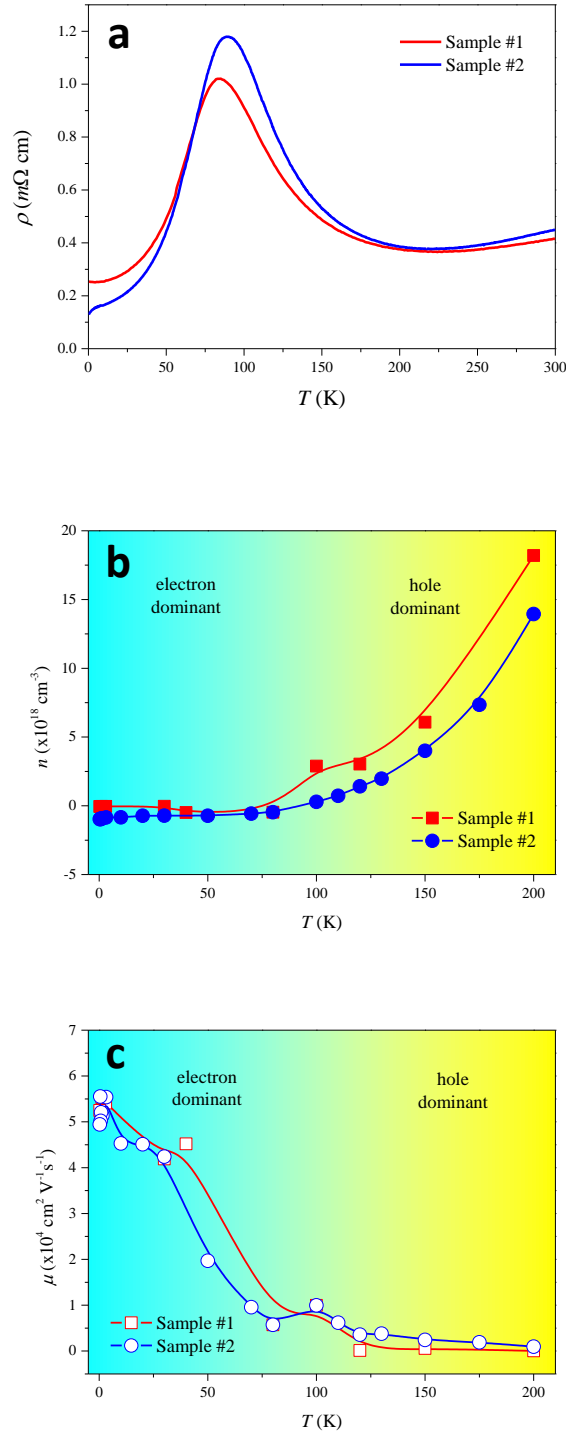


Figure S2. (a) Temperature-dependent electrical resistivity ρ . (b, c) Dominant carrier density n and their mobility μ of ZrTe₅ single crystals. To extract these quantities, a two-band model was used for high temperature data (above 40 K), while the values at low temperature (below 40 K) were taken from the Hall measurement by the linear fitting method.

3. Magnetic field dependent longitudinal thermal resistivity

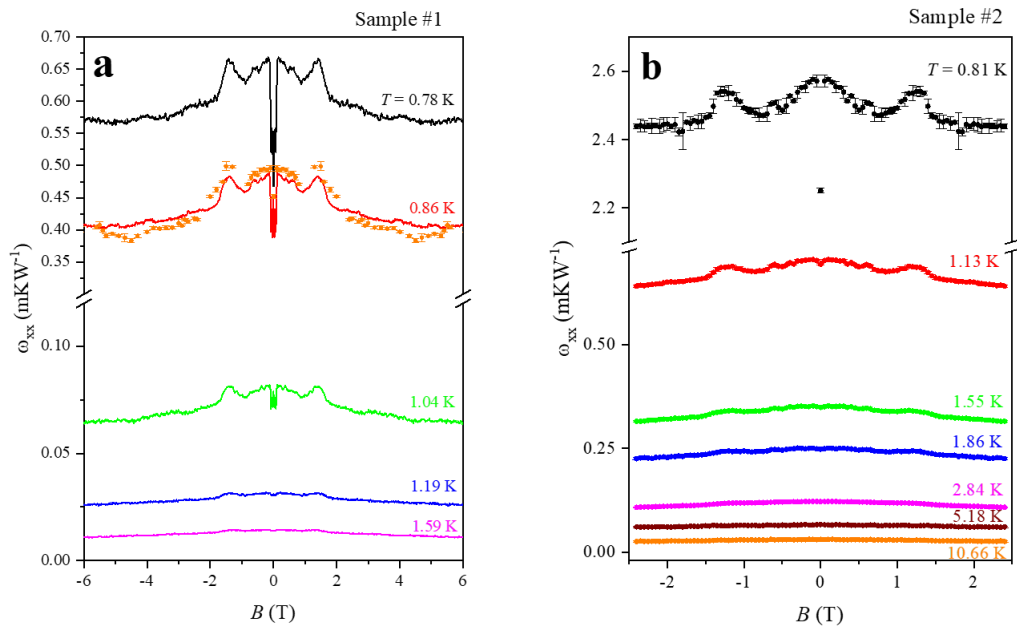


Figure S3. Magnetic field dependent longitudinal thermal resistivity ω_{xx} measured at different temperatures for (a) Sample #1 and (b) Sample #2. We compare two different sweeping B-field modes (continuous and step) at 0.86 K data in (a). Above 80 K data can be found in our previous results [1].

4. Continuous sweep mode thermal Hall angle results for Sample #2

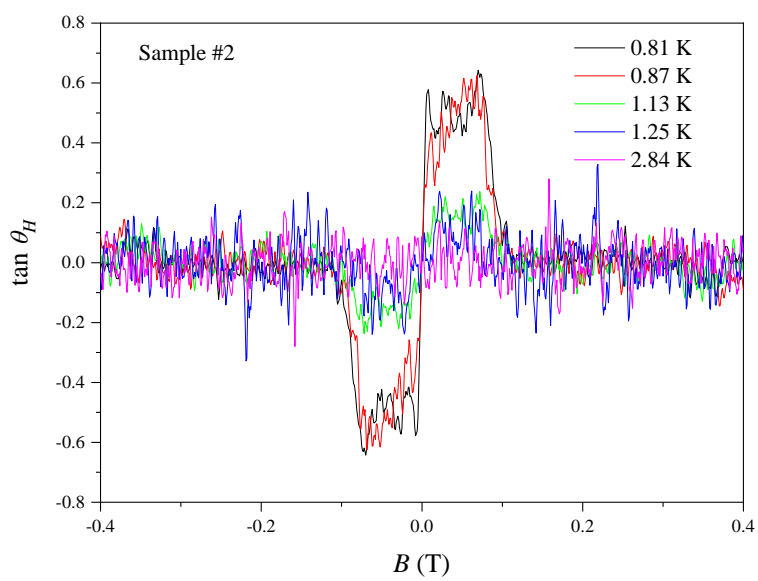


Figure S4. Tangential Hall angle in a narrow magnetic field range with various temperatures for Sample #2.

Supplementary Reference

- [1] P. Wang *et al.*, Physical Review B **103**, 045203 (2021).